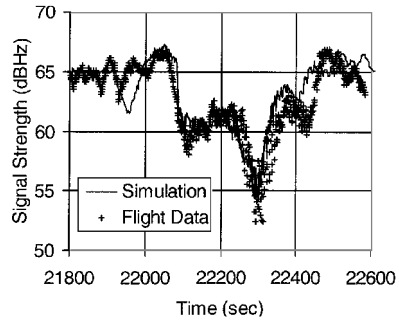

Fig. 3 GTD computed signal strength compared with flight data for S-band low data rate communication link.

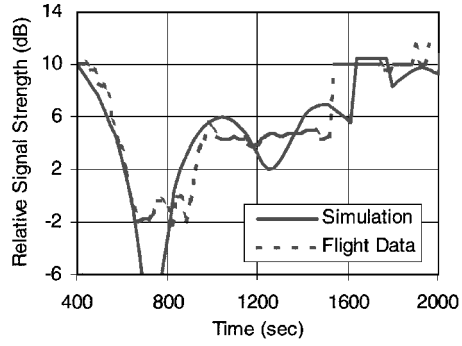

Fig. 4 GTD computed signal strength compared with flight data for S-band high data rate communication link.

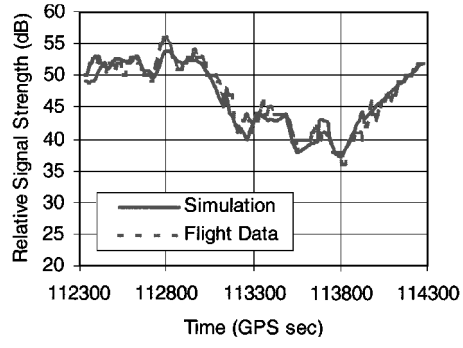

Fig. 5 GTD computed signal strength compared with flight data for selected GPS satellite pass 1.

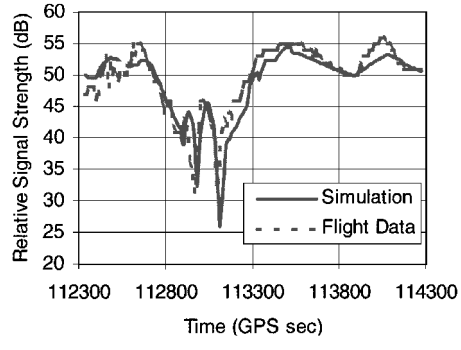

Fig. 6 GTD computed signal strength compared with flight data for selected GPS satellite pass 2.

at a field point r', $\boldsymbol{E}^{r,d}(r')$, can be computed as

$$\boldsymbol{E}^{r,d}(r') = \boldsymbol{E}^{i}(r)\boldsymbol{D}^{r,d}\boldsymbol{A}^{r,d}(s)e^{-jks} \tag{1}$$

where $E^{i}(r)$ is the field incident on the reflection or diffraction point r, $\boldsymbol{D}^{r,d}$ is a dyadic reflection or diffraction coefficient, $\boldsymbol{A}^{r,d}(s)$ is a spreading factor, and s is the distance from the reflection or diffraction point r to the field point r'. $\boldsymbol{D}^{r,d}$ and $\boldsymbol{A}^{r,d}$ can be found from the geometry of the structure at reflection or diffraction point r and the properties of the incident wave there.

Conclusions

The ISS is being assembled in space. Thus, conventional ground tests for communication and navigation system performance are not possible with the ISS completely assembled. Rigorous computer simulations are important for ISS communication and navigation system performance assessment. Both flight data and computer simulation results presented in this Note indicate the solar array panels may be modeled using perfect reflecting plates at S-band frequencies for communication and GPS signal strength predictions.

Reference

[1] Kouyoumijian, R. G., and Pathak, P. H., "A Uniform Geometrical Theory of Diffraction for an Edge in a Perfectly Conducting Surface," *Proceedings of the IEEE*, Vol. 62, No. 11, 1974, pp. 1448–1461.

D. L. Edwards
Associate Editor

Investigation of a Laser-Supported Directed-Energy "Air Spike" in Hypersonic Flow

M. A. S. Minucci,* P. G. P. Toro,† J. B. Chanes Jr.,†
A. G. Ramos,‡ and A. L. Pereira§
IEAv Centro Técnico Aeroespacial,
12228-840 São José dos Campos, São Paulo, Brazil
and
H. T. Nagamatsu¶ and L. N. Myrabo**
Rensselaer Polytechnic Institute,
Troy, New York 12180-3590

Introduction

IT has been suggested by several authors[1–4] that aerodynamic drag and heating of a hypersonic transatmospheric vehicle (TAV) could be greatly reduced by adding energy to the air ahead of it. Such energy addition could be accomplished by focusing a powerful laser or microwave beam ahead of the TAV flight path, as it has been originally suggested by Myrabo and Raizer[2] in 1994.

Myrabo and Raizer called the effect of reducing aerodynamic drag and heating by electromagnetic radiation, the directed-energy "air spike" (DEAS). One of the first experimental confirmation of such an effect came in 1996 when a model of the Apollo reentry

Received 27 April 2001; revision received 30 September 2002; accepted for publication 4 October 2002.

*Major, Brazilian Air Force, Laboratory of Aerothermodynamics and Hypersonics. Senior Member AIAA.

†Research Engineer, Laboratory of Aerothermodynamics and Hypersonics.

‡Research Assistant, Laboratory of Aerothermodynamics and Hypersonics; currently Operational Engineer, Universidade do Vale do Paraíba (UNIVAP), Av. Shishima Hifumi, 2911, 122244-000 São José dos Campos, São Paulo, Brazil.

§Research Assistant, Laboratory of Aerothermodynamics and Hypersonics.

¶Active Professor Emeritus of Aeronautical Engineering, Department of Mechanical Engineering, Aeronautical Engineering, and Mechanics. Fellow AIAA.

**Assistant Professor of Aeronautical Engineering, Department of Mechanical Engineering, Aeronautical Engineering, and Mechanics. Senior Member AIAA.

heat shield fitted with an electric arc plasma torch was tested in the Rensselaer Polytechnic Institute 0.6-m Hypersonic Shock Tunnel by Marsh et al.[5] In these tests the laser focus was represented by air plasma at the tip of the slender plasma torch mounted at the model centerline. It was observed that when the plasma torch was turned on at 35 kW, the conical shock wave, originating at the tip of the torch, would assume a parabolic shape indicating a change in the Mach 10 hypersonic flow caused by the energy addition. Toro extended the DEAS investigation by measuring both the surface-pressure distribution and the surface heat-transfer distribution for several plasma torch power levels.[6,7] The results corroborated Myrabo and Raiser predictions, but the presence of the torch itself made it difficult to completely isolate the torch assembly beneficial effects from those of the energy addition.

The torch assembly had to be eliminated to isolate the effects just mentioned and to simulate the focusing of a laser beam or a microwave beam ahead of the model more closely. Minucci suggested that the energy addition to the flow could be performed by establishing an electric arc between two slender, 1.5-mm-diam, tungsten electrodes mounted at the exit plane of the hypersonic shock-tunnel conical nozzle.[8] The electrodes would be thin enough not to disturb the hypersonic flow and would eliminate the need to use the torch mounting. This experiment is still in progress but has already produced some interesting results.[8,9]

The next natural step constitutes the motivation for the present investigation, which is to use a laser beam to drive the DEAS, as suggested by Myrabo and Raizer. In this situation, the DEAS in front of a vehicle is created by a shock wave propagating from a laser-supported detonation (LSD) wave.

Experimental Apparatus

The laser-supported DEAS experiments were conducted at the Laboratory of Aerothermodynamics and Hypersonics in Brazil. The IEAv 0.3-m Hypersonic Shock Tunnel was used to produce both high- and low-enthalpy hypersonic flow conditions. An excellent description of the facility and its capabilities can be found in Ref. 10. One of the tunnel test-section access windows had to be modified to accommodate the laser-beam delivery system. This system consisted of a 50-mm-diam NaCl lens with a focal distance of 180 mm mounted in a tube. The tube can move inside a support mounted to the test-section window so that the focus can be adjusted to be in the nozzle centerline. Once positioned, the tube, or telescope, is locked in place so that it does not move during the test. Because of geometrical constraints, the telescope had to be positioned at 45 deg with respect to the nozzle centerline. This causes the lens to be damaged frequently and, sometimes, destroyed by high-speed particles/debris that reach the test section at the end of each shock-tunnel run. Also, the energy addition region is not symmetrical with respect to the nozzle centerline because the air plasma, created in the focal point, tends to propagate toward the laser source.[11]

A very simple model consisting of an aluminum hemisphere cylinder, 55-mm diam, was mounted 60 mm downstream of the laser focal point. The model was fitted with one piezoelectric pressure transducer so that the impact pressure downstream of the laser-driven air breakdown could be recorded. The surface of the pressure transducer diaphragm was thermally insulated from flash temperatures by applying two layers of common black vinyl electrical tape. A centerline cylindrical channel, 4.5 mm long and 2 mm in diameter, connected the pressure transducer diaphragm to the model surface.

A transversely excited atmospheric pressure (TEA) carbon dioxide laser, designed and built by Watanuki et al.,[12] was used to drive the DEAS. The laser pulse was synchronized with the shock-tunnel useful test time via a time-delay generator triggered from a piezoelectric pressure transducer, located immediately upstream the nozzle entrance. Three Ge photodiodes were used as light sensors to monitor the generation of the laser pulse inside the laser head (sensor 3), the production of the laser-induced air ignition inside the test section (sensors 1 and 2), and the natural air luminosity of the hypersonic/hypervelocity flow around the model (sensor 2). Two additional pressure transducers, 0.5 m apart, located in the tunnel driven section, were used to time the incident shock wave.

Time-lapse-type photographs of the luminous airflow around the model and of the laser-induced air ignition were taken by using a single-lens reflex camera and ISO 100 color film. In some selected tests a high-speed charge-coupled device (CCD) camera model at 8000 fps and a shutter speed of 1/24,000 s was used to investigate the generation and the extinction of the air ignition in the hypersonic flow. The high-speed camera was triggered simultaneously with the laser pulse and was set with both a pretrigger and a posttrigger acquisition time of 0.5 s.

All of the data, with the exception of the flow visualization, were recorded using a 16-channel 200-kHz data acquisition system. A more detailed description of the apparatus is given in Ref. 13.

Experimental Results and Discussion

The nominal shock-tunnel test conditions are presented in Table 1. These conditions did not vary more than 5% from run to run. The laser operating conditions can be found in Table 2.

From Table 1 it is quite evident that the static pressures present in the hypersonic flow at the nozzle exit were quite low. As a consequence, the authors expected some difficulty in inducing air ignition[11] considering laser energy available, shown in Table 2. However, it was experimentally observed that, for the high-enthalpy runs, laser-induced air breakdown would always take place in the low-pressure conditions existing in the hypersonic flow upstream of the model. At first the present authors were led to believe that the air ignition was being triggered by particles/debris contaminating the flow.

Once the low-enthalpy tests were performed and the laser-induced air breakdown could not be established as in the high-enthalpy case,[13] the particle contamination idea became uncertain.

Because air was used in both high- and low-enthalpy tests, any contaminants that could trigger the air ignition were present in both scenarios. The authors suspect that probably a combination of a high static temperature, 1000 K, and nonequilibrium effects present in the flow could be responsible for the successful laser-induced air ignition at these low static pressures.

Figure 1 shows the impact pressure trace and the output traces from light sensors 1 and 3. Light sensor 3 clearly indicates the moment the TEA laser fired by recording the luminosity coming out from the laser cavity electric discharge. On the other hand, the natural air luminosity of the hypervelocity flow around the model, as well as the luminosity of the laser-induced air breakdown, can be seen in the output trace from light sensor 1.

Interestingly enough, the impact pressure trace seems to show the effect of the laser-induced air breakdown. Shortly after the air ignition is generated, a high-frequency "ringing" indicates the impact of the detonation wave against the model front surface, and a drop in pressure occurs. This drop in the impact pressure coincides with the duration of the air ignition and might indicate a decrease in the aerodynamic drag caused by the DEAS effect. However, these results are preliminary, and additional tests and analysis are necessary.

A time-lapse-type photograph of the laser-induced air ignition in the Mach 6.2 flow for high-enthalpy reservoir conditions can be

Table 1 Shock-tunnel test-conditions

Parameter	High enthalpy	Low enthalpy
Reservoir pressure, bar	120.0	25.0
Reservoir temperature, K	5000.0	950.0
Reservoir enthalpy, MJ/kg	9.0	1.0
Freestream pressure, mbar	12.0	4.0
Freestream temperature, K	1000	77.0
Freestream density, g/m^3	4.0	17.0
Freestream Mach number	6.2	7.8

Table 2 CO_2 TEA laser operating conditions

Condition	Value
Energy per pulse, J[a]	7.5
Pulse duration, ns	120
Gas mixture	7%CO_2-54%N_2-39%He

[a]Average between the energy meter readings immediately before and after the test.

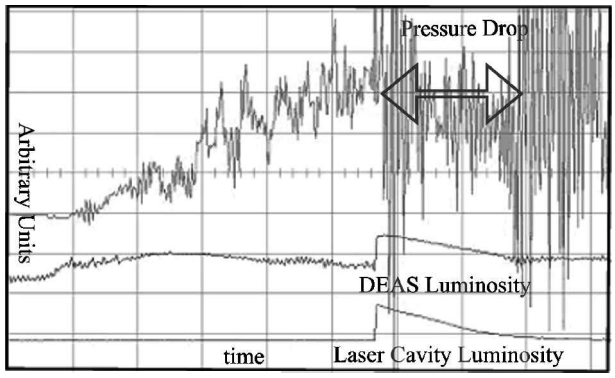

Fig. 1 Typical high-enthalpy impact pressure (top), light sensor 1 (middle), and light sensor 3 (bottom) traces.

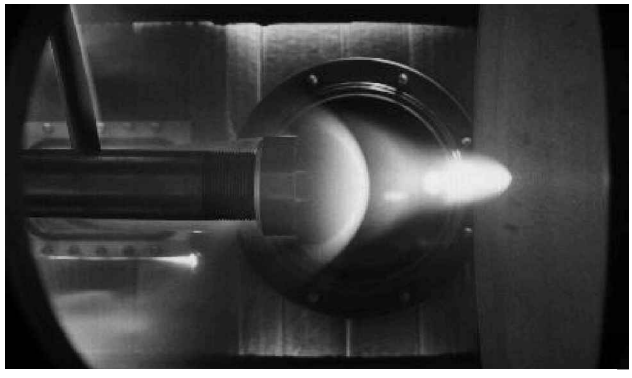

Fig. 2 Open-shutter photograph of the laser-induced air ignition in Mach 6.2 flow and of the strong normal and weak conical shock waves in front of the model.

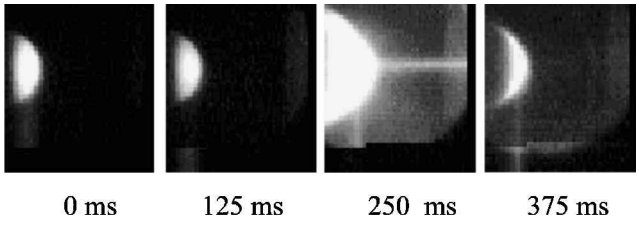

Fig. 3 Time history of the generation and extinction of the laser-supported DEAS in high-enthalpy flow.

seen in Fig. 2. Both the bow shock wave and the conical flow structure, upstream of the model, are superimposed in this photograph. Because of stray light, it is also possible to see internal details of the test section, the sting mounting, the nozzle exit, and even the infrared telescope mounting behind the sting.

The conical flow structure seen in Fig. 2 seems to agree with the impact pressure drop observed in Fig. 1 and also via the DEAS mechanism proposed by Myrabo and Raizer.[2] As soon as the laser-induced air breakdown develops, the free-stream air is pushed by the LSD wave from the region immediately upstream of the model. Consequently the impact pressure decreases, and the flow is pushed over the air spike to the periphery of the hemisphere generating the conical flow structure seen in Fig. 2. This conical flow structure creates a detached conical shock wave (parabolic-shaped) well ahead of hemisphere.

Additional information on the dynamics of the establishment of the DEAS came with the utilization of a high-speed camera. Figure 3 shows a sequence of frames taken every 125 μs and an exposure time of 1/24,000 s. From the sequence of frames depicted, one can see that the bow shock is established over the hemisphere-cylinder model until the laser-induced air ignition creates the DEAS at 250 μs, and the shock wave becomes conical. After that, when the air ignition is extinguished at 375 μs the bow shock structure is reestablished. This behavior agrees with the trend observed in the high-enthalpy impact pressure trace (Fig. 1) in which the pressure decreases shortly after the establishment of the air breakdown and increases when ignition is extinguished.

Conclusions

Preliminary experiments to demonstrate the laser-supported DEAS concept in Mach 6.2 flow (real air) and Mach 7.8 flow (ideal air) were conducted in the IEAv 0.3-m Hypersonic Shock Tunnel. A CO_2 TEA laser was used to drive the air ignition upstream of a hemisphere cylinder installed in the modified shock-tunnel test section. It was observed that, for high-enthalpy reservoir conditions, laser-induced air ignition could be established consistently in spite of the low static pressures present in the hypersonic airflow. A piezoelectric pressure transducer, installed in the model, indicated a drop in the impact pressure that coincided with the duration of the luminosity generated by the laser-induced air breakdown. Time-lapse-type photographs have shown a conical flow structure superimposed to the bow shock wave standing in front of the hemisphere cylinder. The dynamics of the formation of the conical flow structure was revealed through the use of a high-speed CCD camera. The frames show the initial bow shock in front of the hemisphere, followed by a conical flow structure at the moment of the laser-induced air ignition, which transforms back into the bow shock when the ignition is extinguished. These preliminary results seem to indicate that the laser-induced air breakdown was indeed generating a directed-energy air spike, and this effect reduced the impact pressure on the model. Low-enthalpy, ideal air, runs were also performed, but the laser-supported air ignition could not be established either consistently or completely.

Acknowledgments

The financial support received from Fundação de Apoio à Pesquisa do Estado de São Paulo through Grant 2000/11792-5 is acknowledged. The authors express their gratitude to Nicolau A. S. Rodrigues, Antônio O. Toledo, Antônio C. Oliveira, and Laurentino C. V. Neto for their invaluable support and advice. The authors are also in debt to André Jacobovitz and Lincon T. Tan, from LYNX Com. Imp. Ltda., for the technical support and graceful use of the high-speed change-coupled device camera.

References

[1] Tidman, D. A., "Apparatus and Method for Facilitating Supersonic Motion of Bodies Through the Atmosphere," U.S. Patent 4,917,335, April 1990.

[2] Myrabo, L. N., and Raizer, Yu. P., "Laser Induced Air Spike for Advanced Tansatmospheric Vehicles," AIAA Paper 94-2451, June 1994.

[3] Gurijanov, E. P., and Harsha, P. T., "AJAX: New Directions in Hypersonic Technology," AIAA Paper 96-4609, Nov. 1996.

[4] Covault, G., "'Global Presence' Objective Drives Hypersonic Research," *Aviation Week and Space Technology*, Vol. 150, No. 4, 1999, pp. 54–58.

[5] Marsh, J. J., Myrabo, L. N., Messitt, D. G., and Nagamatsu, H. T., "Experimental Investigation of the Hypersonic 'Air Spike' Inlet at Mach 10," AIAA Paper 96-0721, Jan. 1996.

[6] Toro, P. G. P., Nagamatsu, H. T., Minucci, M. A. S., and Myrabo, L. N., "Experimental Pressure Investigation of a 'Directed-Energy Air Spike' Inlet at Mach 10," AIAA Paper 99-2843, July 1999.

[7] Toro, P. G. P., Nagamatsu, H. T., Myrabo, L. N., and Minucci, M. A. S., "Experimental Heat Transfer Investigation of a 'Directed-Energy Air Spike' Inlet at Mach 10," AIAA Paper 99-2844, July 1999.

[8] Minucci, M. A. S., Bracken, R. M., Myrabo, L. N., Nagamatsu, H. T., and Shanahan, K. J., "Experimental Investigation of an Electric Arc Simulated 'Air Spike' in Hypersonic Flow," AIAA Paper 00-0715, Jan. 2000.

[9] Bracken, R. M., Myrabo, L. N., Nagamatsu, H. T., Meloney, E. D., and Minucci, M. A. S., "Arc Simulated 'Air-Spike' in the RPI Hypersonic Shock Tunnel at Mach 10 and Arc Powers up to 11 MW," 7th International Workshop on Shock Tube Technology, GASL, Inc., Sept. 2000.

[10] Nascimento, M. A. C., "Gaseous Piston Effect in Shock Tube/Tunnel When Operating in the Equilibrium Interface Condition," Ph.D. Dissertation, Dept. of Aeronautical Engineering, Inst. Tecnológico de Aeronáutica, São José dos Campos, Brazil, Oct. 1997.

[11] Raizer, Y. P., *Laser-Induced Discharge Phenomena*, Studies in Soviet Science, Consultants Bureau, New York, 1977, pp. 63–102.

[12] Watanuki, J. T., Oliva, J. L. S., Lobo, M. F. G., and Rodrigues, N. A. S., "Laser de CO_2-Híbrido com Célula de Baixa Pressão Pulsada," *Revista de Física Aplicada e Instrumentação*, Vol. 3, No. 3, 1988, pp. 207–216 (in Portuguese).

[13] Minucci, M. A. S., Toro, P. G. P., Chanes, J. B., Jr., Ramos, A. G., Pereira, A. L., Nagamatsu, H. T., and Myrabo, L. N., "Investigation of a Laser-Supported Directed-Energy 'Air Spike' in Mach 6.2 Air Flow — Preliminary Results," AIAA Paper 2001-0641, Jan. 2001.

T. C. Lin
Associate Editor

Plume Interference Effects on Missile Bodies

S. Raghunathan,* H. D. Kim,† and E. Benard‡
Queen's University Belfast,
Belfast, Northern Ireland BT9 5AG, United Kingdom
and
P. Mallon§ and R. Harrison¶
Thales Defence, Ltd.,
Belfast, Northern Ireland BT6 9HB, United Kingdom

Nomenclature

C_p = pressure coefficient, $(p - p_\infty)/(\frac{1}{2}\rho_\infty V_\infty^2)$
M_∞ = freestream Mach number
P_c = total pressure at the combustion chamber
p = local pressure
p_a = freestream static pressure
V_∞ = freestream velocity
x = axial distance
ρ_∞ = freesteam density

Introduction

IN recent years, there has been considerable progress in propulsion technology for supersonic flight bodies. The development of missile powerplants that produce high thrust density (ratio of thrust to reference cross-sectional area) has introduced several missile aerodynamic problems. These include degradation of longitudinal stability, reduced control effectiveness, and induced yawing moments, largely due to the strong interaction between an underexpanded exhaust plume and the boundary layer along the missile body surface.[1–6]

The interaction between a supersonic freestream and plume on a missile body[2,3] is typified in Fig. 1. Jet expansion at the nozzle exit produces a deflection of the external freestream flow and generates a rise in pressure, partially communicated upstream through the viscous layer very close to the body surface. In supersonic external flows, this nearly always leads to a series of oblique compression waves. For large jet-to-freestream pressure ratios, the compression waves coalesce to form a strong shock wave, leading to boundary-layer separation forward of the base. The supersonic plume is generated by the interaction of an imperfectly expanded supersonic jet with its surrounding conditions and has a number of distinct flow regions with different characteristic features.

For large jet pressure ratios, as experienced in missile systems, the plume is often characterized by an inviscid barrel shock cell structure, with shear layers developing along the plume and Mach disks. Embedded zones of subsonic flow occur just behind the Mach disks, and slipstreams generate from the triple point of the Mach disk and the barrel shocks, whereas a significant portion of the plume mixing layer may be subsonic even for jets exhausting into supersonic external freestream. This is due to the plume-induced shock on the missile body.

The plume-induced shock can lead to plume-induced separation, involving interaction between the separated shear layers, the shock waves, and the boundary layer. It is essential to have a detailed understanding of these interactions for an effective design of tactical missiles, but such an understanding is lacking at present. This Note presents research investigations directed toward a better understanding of the complex flow features over a missile body.

Computational Analysis

Computational fluid dynamic (CFD) studies were performed for simple missile configurations, namely, a cone cylinder (Fig. 2) and an ogive cylinder, with and without the exhaust plume. The model had a length L of approximately 1000 mm (varied slightly for comparison with the wind-tunnel data) and diameter D of 40 mm. The ogive-cylinder cone length of the model l was 240 mm (Fig. 3).

A commercially available code, Fluent 5, that is the most capable of analyzing the complex compressible flows around the missile body was used. The code has the ability to predict the flowfields involving strong shock interactions with shear layers and boundary layers.

Fluent 5 uses a fully implicit finite volume method to solve either the Euler or the Navier–Stokes equations. For the viscous turbulent flow analysis, two-equation turbulent stress models, standard k–e and renormalized group (RNG) k–e, which were modified to take account for compressibility effect, are employed to close the governing equations.

In the present computations, structured grids were employed for the simple missile configuration. With respect to temporal discretization, an explicit multistage time-stepping scheme is used to discretize the time derivatives in the governing equations. Using a second-order-accurate scheme with fine computational grids in the vicinity of the shock and wake flow makes it feasible to capture the shock structure near the forebody, as well as the wake flow downstream of the afterbody, of the missile model. The computational effort of effectively capturing them was reduced in the present computations by using an adaptive finite volume grid algorithm.

A multigrid scheme was used to accelerate the convergence of the solution on a series of coarse grid levels. The net mass flux through the computational boundaries was investigated to determine if there was an applicable imbalance through the boundaries.

In the case of the computations of the plume interference, the computational domain strongly affects the solutions obtained. With a high plume pressure ratio, the computational boundary downstream should be extended sufficient to reduce the high pressure of the plume to atmospheric conditions. In the present computations, the domain was extended about $40L$ upstream from the missile model and about $120L$ downstream away from the missile body.

The pressure far-field boundary conditions were used to simulate freestream conditions at infinity, with the inlet and outlet boundaries providing the requisite flow conditions. In addition to the model wall and the symmetry boundary conditions, the pressure inlet along the upstream boundary, the pressure outlet along the downstream boundary, and the pressure far-field on the sidestream boundary can specify another set of boundary conditions.

In the current computations, freestream Mach number M_0 was varied in a range of low supersonic flow speeds. Freestream static pressure and temperatures were kept constant 101325.1 Pa and 288.15 K, respectively, as is typical in wind-tunnel test flows. These conditions result in Reynolds number based on the model length from 2.0×10^7 to 4.5×10^7. The plume pressure ratio, defined as the ratio P_c/p_a of total pressure P_c at the combustion chamber to freestream static pressure p_a, was varied in the range

Received 8 March 2001; revision received 15 August 2001; accepted for publication 7 December 2001.

*Professor and Head of School, School Aeronautical Engineering. Associate Fellow AIAA.
†Senior Visiting Fellow, School Aeronautical Engineering. Member AIAA.
‡Lecturer, School Aeronautical Engineering.
§Senior Team Manager, Aerodynamics.
¶Director of Engineering, Future Research.